Photoinduced Vibrational Coherence Transfer in Molecular Dimers†

Dmitri S. Kilin,‡ Oleg V. Prezhdo,*,‡ and Michael Schreiber§

Department of Chemistry, University of Washington, Seattle, Washington 98195-1700, and Institut für Physik, Technische Universität Chemnitz, D-09107 Chemnitz, Germany

Received: February 1, 2007; In Final Form: May 24, 2007

At short times that are faster than dephasing, photoinduced evolution of the vibrational subsystem in an electron−phonon molecular structure depends strongly on the electronic evolution. As the electronic population shifts between the donor and acceptor states, in the diabatic description the state with the largest population determines the equilibrium positions and frequencies of the vibrational modes, which oscillate continuously and without loss of coherence. The vibrational coherence transfer between the electronic states detected recently in a number of systems is described theoretically by application of the quantized Hamiltonian dynamics (QHD) formalism [*J. Chem. Phys.* **2000**, *113*, 6557] to the coupled electronic and vibrational degrees of freedom of a model heterodimer. The observed coherent modulation of the frequency of the probe signal is represented with simple analytic and numeric QHD models.

1. Introduction

The need for novel energy sources drives the design of artificial light-harvesting systems. Understanding the extremely efficient use of solar energy seen in nature and formulation of the basic principles of energy transfer in the artificial complexes pose multiple theoretical challenges. Important examples include the sequence of energy- and electron-transfer events that determine collection and storage of solar energy in the bacteriochlorophyll units of the natural light-harvesting antennae,[1−9] and the femtosecond electron dynamics in artificial solar cells composed of inorganic semiconductor substrates sensitized with molecular chromophores.[10−19] The desired transfer processes in such systems are driven by the ultrafast photoinduced evolution of the electronic degrees of freedom that are strongly affected by the dynamic reorganization of the quantized vibrational modes.[20−24] Theoretical description of the transfer processes that are responsible for the natural and artificial light harvesting requires explicit modeling of the coupled electronic and vibrational dynamics together with bath-induced dephasing and renormalization of system energies.[22−29]

Conceptual approaches to the description of electronic dynamics were developed for photoinduced evolution of electronic degrees of freedom leading to both energy and electron transfer. The long-range energy (exciton) transfer between chromophores in molecular aggregates is well described by the Förster theory,[30] where the transfer is also assumed to take place after thermalization of the vibrational degrees of freedom. The transfer rate in the Förster theory is proportional to the overlap of the donor emission and acceptor absorption spectra. The Förster theory successfully describes the enhancement of absorption efficiency in the networks of chromophores acting as solar radiation antennas.[1−3] The Marcus theory[31−34] provides a standard framework for the description of electron transfer (ET). It is a transition state theory that assumes rapid thermalization of vibrational levels of the reactant relative to the transfer rate[34−36] and does not consider explicit quantum dynamics. The theory accounts for nonadiabatic ET by correcting the transfer rate for weak donor−acceptor coupling and shows that ET models should take into account both electronic and vibrational sublevels.

Ultrafast transfer processes require the calculation of explicit quantum dynamics, in particular, for those degrees of freedom that are not thermalized on the time scale of the transfer.[34−36] The reduced density matrix methods[9−11,24−26,37,38] provide a consistent framework for a quantum treatment of several explicit electronic and vibrational modes that are coupled to a thermal bath of many modes. The master equations derived for the reduced density matrices may be cast in certain limits into the form of quantum jump equations[39−43] that deal with individual trajectories rather than ensembles. Although the reduced density matrix description is fully quantum mechanical, its application is not straightforward if the bath experiences a strong feedback due to changes in the main system. For instance, the redistribution of charge in ET reactions can significantly alter the electrostatic interactions seen in the electron donor and acceptor configurations. Generating large reorganization energies, modifications of the solvation structure are well treated at the classical level by molecular dynamics techniques.[44−49] The need to study dynamics of mixed quantum-classical models, composed of a few quantum mechanical electronic and vibrational modes that are coupled to explicit classical degrees of freedom has resulted in a family of approaches, among which Tully's surface hopping[50] is a well-known representative.

The current paper uses the quantized Hamiltonian dynamics (QHD) formalism,[51−60] which starts with the Heisenberg formulation of quantum mechanics and leads to a hierarchy of approximations representing higher order expectation values by products of the lower order variables. The QHD approach captures many quantum properties with a computational effort similar to that for classical dynamics. Originally developed for vibrational degrees of freedom,[51,53−56,58−60] the method was extended to systems involving both vibrational and electronic

† Part of the special issue "Robert E. Wyatt Festschrift".

* Corresponding author. E-mail: prezhdo@u.washington.edu.
‡ University of Washington.
§ Technische Universität Chemnitz.

10.1021/jp0709050 CCC: $37.00
Published on Web 09/13/2007

modes.[52,57] Applied to ET, QHD analytically reproduced multiple periods of the ultrafast electronic population transfer and its vibrationally induced dephasing.[57] Here, the QHD description of ET is extended to the vibrational coherence transfer that has provided signatures of nontrivial quantum dynamics in recent pump−probe experiments.[20−24,61−65] The presented vibronic model of a heterodimer includes donor and acceptor electronic states with vibrational substructure and captures many key properties of the ET dynamics observed in such systems as bacteriochlorophyll aggregates[5,6,22,62] and dye-semiconductor solar cells.[9−19]

The transfer of vibrational coherence occurs faster than vibrational thermalization and can be detected if the length of the optical pulse is shorter than the vibrational period.[66] For instance, the oscillations seen in the stimulated emission spectra and excited-state absorption of the bacteriochlorophyll dimer P* indicated that vibrational coherence can persist for several picoseconds following a short-pulse excitation.[7,41,67,68] Short laser pulses revealed coherence transfer associated with high-frequency modes,[7] up to 1000 cm^{-1}. These long-lasting coherence effects suggest intriguing new types of excited-state dynamics. This paper focuses on the tendency of the vibrational coherence to outlive the transfer process and to reflect the properties of both donor- and acceptor-state energy surfaces through the time-resolved spectroscopic signal.

The persistence of the vibrational coherence for times longer than the transfer time can have two effects. In systems with large reorganization energies and small donor−acceptor coupling, the vibrational coherence modulates the transfer process as in the ET from the special reaction center pair P* to bacteriopheophitin[4] ($P^*B_A^-$) or in the dye-sensitized semiconductors.[14] The transfer proceeds in a stepwise manner, with a small amount of the acceptor wavepacket formed each time the donor wavepacket approaches the interaction region. In the opposite case of small reorganization energy and large donor−acceptor coupling, the electron or energy transfer modulates the vibrational coherence. The whole vibrational wavepacket moves between the electronic energy surfaces, changing its vibrational frequency, but preserving its phase. The effect of the electronic evolution on the vibrational dynamics is discussed here in detail.

The paper is organized as follows. Section 2.1 introduces the model and defines the quantum-mechanical operator for the observable probe signal. Section 2.2 presents the Hamiltonian that drives the transfer dynamics. The equations of motion for the coherences and important auxiliary observables are derived in section 2.3. Section 2.4 gives the approximate solutions for the evolution of the coherences obtained by the QHD approach with simple closure. The results are presented in section 3. The dynamic features of the coherences are discussed in section 3.1. The connection between the coherences and the probe signal is presented in section 3.2. The dynamics of the probe signal and manifestations of the coherence transfer are analyzed in section 3.3. The concluding section summarizes the key results of the paper, stressing the significance of the vibrational coherence transfer relative to the more common transfer of electronic energy and population.

2. Theory

2.1. Quantum-Mechanical Observable of the Probe Signal. Consider an optically active vibrational mode that is triggered by an electronic excitation. In a number of recent experiments,[6,20,23,61] including the pump−probe studies of bacteriochlorophyll aggregates,[62] the probe signal was strongly modulated by such a vibrational mode. The frequency of the mode evolved over time. Figure 1a describes this effect. The pump pulse promotes the ground-state vibrational wavepacket to one of the two optically active excited states. The wavepacket then moves to the other excited state driven by ET. The probe signal W is determined by the energy difference between the excited-state and ground-state potential energy surfaces evaluated at the current location of the vibrational wavepacket q. In particular, $W = U_1(q) - U_f(q)$ for the excitation localized in the excited state $|1\rangle$, and $W = U_{1'}(q) - U_f(q)$ for the excitation localized in the excited state $|1'\rangle$. The final state $|f\rangle$ can be either the ground state $f = 0$, as in a pump−dump scheme, or a doubly excited state $f = 2$, as in a transient absorption scheme. Because the relevant evolution of the vibrational wavepacket occurs between states $|1\rangle$ and $|1'\rangle$, without loss of generality and for simplicity, we consider $f = 0$. The energy of the probe signal is modulated by the vibrational motion.

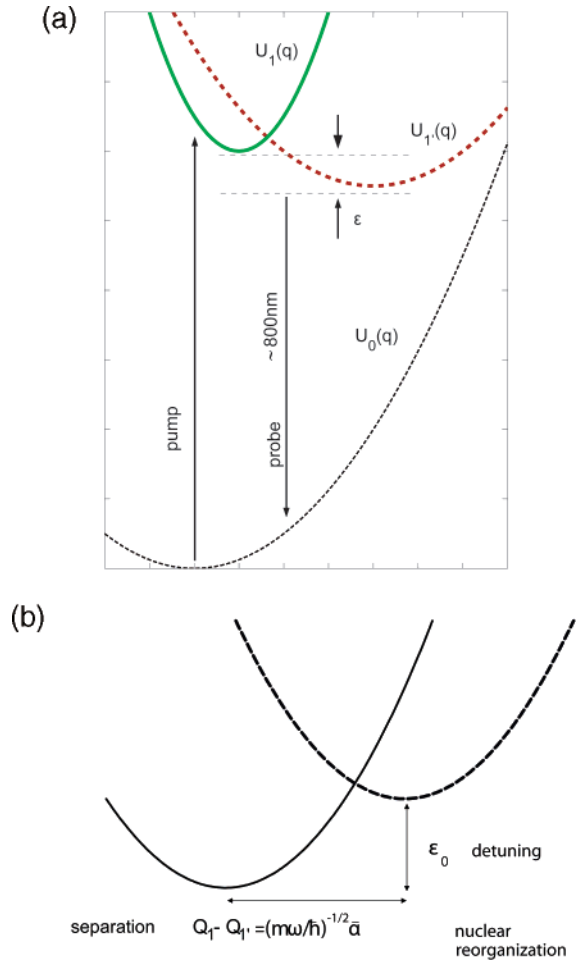

Figure 1. Potential energy surfaces involved in the vibrational coherence transfer. (a) Measurement of vibrational coherence transfer in bacteriochlorophyll.[62] The pump pulse (arrow up) promotes the vibrational wavepacket from the electronic ground state $|0\rangle$ with potential $U_0(q)$ (short dashes) to the excited electronic state $|1\rangle$ with a steeper potential $U_1(q)$ (solid line), eq 1. Upon photoexcitation, the wavepacket may transfer to the second excited state $|1'\rangle$ with a softer potential $U_{1'}(q)$ (long dashes). Depending on the location of the wavepacket, the probe signal (arrow down) is modulated by one (ω_1) or the other ($\omega_{1'}$) vibrational frequency. (b) Simplified model for the vibrational coherence transfer. The potential energy surfaces are associated with the initial $|1\rangle$ (solid line) and final $|1'\rangle$ (dashes) excited electronic states.

The vibrational potential energy surfaces associated with the electronic states are

$$U_1(q) = m\omega_1{}^2(q - Q_1)^2/2 + \epsilon_{10}$$
$$U_{1'}(q) = m\omega_{1'}{}^2(q - Q_{1'})^2/2 + \epsilon_{1'0}$$
$$U_0(q) = m\omega_0{}^2q^2/2 \quad (1)$$

Here, ϵ_{10} and $\epsilon_{1'0}$ are the electronic energy differences between the ground and two excited states. Generally, each potential in eq 1 is characterized by its own frequency ω_1, $\omega_{1'}$, or ω_0 and equilibrium value Q_1, $Q_{1'}$, or 0 of the vibrational coordinate q. The continuity in the vibrational evolution during the ET produces a nontrivial phenomenon known as the vibrational coherence transfer.[6,20,23,61] The phenomenon becomes possible only if the vibrational motion along the ET coordinate is decoupled from the environment, such that the latter cannot significantly perturb the vibrational evolution on the ET time scale. The vibrational coherence transfer can be most easily detected experimentally if the donor and acceptor potential energy surfaces are characterized by different frequencies, $\omega_1 \neq \omega_{1'}$. Then, the frequency of the modulation of the experimental signal depends on the curvature of the potential, which is occupied at a given time.

The vibrational coherence transfer can be detected in the experimental signal, even if the donor and acceptor surfaces have the same curvature. Identifying the populations of the electronic states with the projection operators $|1\rangle\langle 1|$ and $|1'\rangle\langle 1'|$, the probe signal operator can be expressed as follows

$$W = (U_1(q) - U_0(q))|1\rangle\langle 1| + (U_{1'}(q) - U_0(q))|1'\rangle\langle 1'| \quad (2)$$
$$= |1\rangle\langle 1|\{\epsilon_{10} + m(\omega_1{}^2 - \omega_0{}^2)q^2/2 - m\omega_1{}^2qQ_1 + m\omega_1{}^2Q_1{}^2/2\} + |1'\rangle\langle 1'|\{\epsilon_{1'0} + m(\omega_{1'}{}^2 - \omega_0{}^2)q^2/2 - m\omega_{1'}{}^2qQ_{1'} + m\omega_{1'}{}^2Q_{1'}{}^2/2\}$$

If the potential energy surfaces have equal curvatures $\omega_1 = \omega_{1'} = \omega_0 = \omega$, and the excitation energies are the same $\epsilon_{10} = \epsilon_{1'0} = h\nu_0$, the dynamical contribution to the signal arises from the state-specific coordinate operators $q|1\rangle\langle 1|$ and $q|1'\rangle\langle 1'|$ that contribute to the change of the transition energy

$$W = h\nu_0 - m\omega^2(q|1\rangle\langle 1|Q_1 + q|1'\rangle\langle 1'|Q_{1'}) \quad (3)$$

The terms containing the state-specific coordinate operators modulate not only the signal energy, but also its amplitude, because, in general, the optical transitions involving states $|1\rangle$ and $|1'\rangle$ have different intensities. The vibrational coherence transfer can also be detected by polarization measurements of transitions involving the two electronic states.

The vibrational coherence transfer is determined by the excited-state dynamics and can be studied with a scheme shown in Figure 1b. The coherence transfer phenomenon is described below by a simple analytic model.

2.2. The Model Hamiltonian. The model includes two electronic states $|1\rangle$, $|1'\rangle$ and a nuclear degree of freedom q represented by a harmonic oscillator, whose frequency is independent of the electronic state $\omega_1 = \omega_{1'} = \omega$. The electronic Hamiltonian is defined by the site energy ϵ and coupling J, which are both dependent on the nuclear coordinate $q = \sqrt{\hbar/2m\omega}(a^+ + a)$:

$$H_{el-ph} = \hbar\omega\,(a^+a + 1/2) + \epsilon(q)S_+S_- + J(q)\,(S_+ + S_-) \quad (4)$$

Here, $S_- = |1\rangle\langle 1'|$ and a are the lowering operators of the electronic and vibrational subsystems, respectively. These operators represent quantum coherence effects. The expectation values of S_- and a are nonzero only if there is quantum correlation between the upper and lower states. The S_- and a operators will be referred to throughout the paper as the coherence operators.

The dependence of the site energy and coupling on the nuclear configuration is modeled by the leading order in the Taylor expansion. Note that the quadratic returning potential is already included in the phonon Hamiltonian. The interaction between the electronic and vibrational subsystems is taken here in the first order (bilinear) approximation.[57,69]

$$\epsilon(q) = \epsilon_0 + \epsilon'_q q$$
$$J(q) = J_0 + J'_q q \quad (5)$$

The expansion accounts for the fact that the equilibrium nuclear positions may and usually will differ for the two electronic states. The Hamiltonian becomes

$$H_{el-ph} = \underbrace{\hbar\omega[a^+a + 1/2]S_-S_+}_{\text{lower surface}} + \underbrace{\hbar\omega[(\alpha^+ + \bar{\alpha}^*)(\alpha + \bar{\alpha}) + 1/2]S_+S_-}_{\text{upper surface}} + \underbrace{[J_0 + g(a + a^+)](S_+ + S_-)}_{\text{coupling}} + \underbrace{(\epsilon - \hbar\omega\bar{\alpha}^*\bar{\alpha})S_+S_-}_{\text{detuning}} \quad (6)$$

where $g = \sqrt{\hbar/2m\omega}J'_q$ stands for the coupling strength, and $\bar{\alpha} = (Q_{1'} - Q_1)\sqrt{m\omega/2\hbar}$ is the dimensionless difference of the equilibrium positions, Figure 1b. If the nuclear reorganization energy $\hbar\omega\bar{\alpha}^*\bar{\alpha} = m\omega^2(Q_1 - Q_{1'})^2/2$ is small compared to the number of vibrational excitation quanta, the Hamiltonian (6) takes the form

$$H = \hbar\omega a^+a + \hbar\Omega S_+S_- + g(a^+ + a)(S_+ + S_-) \quad (7)$$

where $\Omega = \epsilon_0/\hbar$. Small nuclear reorganization energy corresponds to a small Huang−Rhys factor that is typical of stiff systems, such as quantum dots,[70−72] carbon nanotubes[73−75] and molecular donor−acceptor species connected by rigid bridges.[76,77]

The dynamics of the model system is studied within the QHD approach.[51−60] In particular, an approximate closed analytic time dependence of the expectation value of the excited-state population difference operator $S_z = (|1'\rangle\langle 1'| - |1\rangle\langle 1|)/2$ has been obtained in ref 57

$$\langle S_z\rangle \approx -\frac{1}{2} + \frac{g^2\sqrt{\gamma_1}\left[\sqrt{\gamma_1} + 1\right]}{2\omega_a{}^2}(1 - \cos\omega_a t) + \frac{g^2\sqrt{\gamma_1}\left[\sqrt{\gamma_1} - 1\right]}{2\omega_b{}^2}(1 - \cos\omega_b t) \quad (8)$$

and is illustrated in Figure 2. The evolution of $\langle S_z\rangle(t)$ is used below to construct the dynamics of vibrational coherence. Generally, the current level of the QHD approximation remains valid up to the first dephasing of the electronic population, $t\omega/(2\pi) \simeq 50$ in Figure 2. This criterion remains valid for a wide range of the electron−phonon coupling and initial conditions. The values were chosen in Figure 2 to

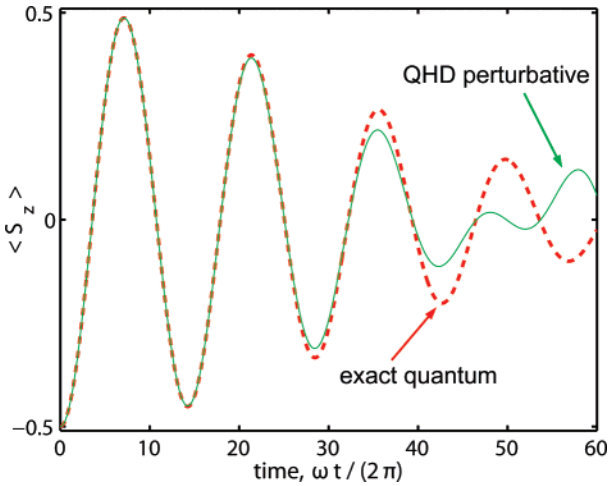

Figure 2. Time dependence of the electronic population $\langle S_z \rangle$. The expectation value $\langle S_z \rangle$ is computed by exact numeric diagonalization of Hamiltonian (7) (red dashes) and approximately using eq 8 (green solid line), for weak coupling $g = 0.005$ and large vibrational amplitude $\langle a^+a \rangle_{t=0} = 49$. $(S_z)_{t=0} = -1/2$, and $\delta = 0$. The population oscillates with a high frequency ω_+ and displays quasirelaxation on a slower time scale determined by ω_-, where $\omega_\pm = 1/2(\omega_a \pm \omega_b)$ and $\omega_{a,b}$ are defined in eq 9. Good agreement between the exact and approximate solutions is observed during the first several periods of the population inversion.

allow for several oscillations of the electronic population prior to the population dephasing.

The oscillation frequencies ω_a, ω_b

$$\omega_a{}^2 = \delta^2 + 2g^2(\gamma_1 + \sqrt{\gamma_1})$$
$$\omega_b{}^2 = \delta^2 + 2g^2(\gamma_1 - \sqrt{\gamma_1}) \qquad (9)$$

where

$$\gamma_1 = \langle a^+a \rangle + \langle S_z \rangle + 1/2$$
$$\delta = \Omega - \omega$$

depend on the difference in the electronic and vibrational frequencies δ and the number of the vibrational excitation quanta $\langle a^+a \rangle$. The expectation value γ_1 is a constant of motion of Hamiltonian (7). Assuming without loss of generality that the electronic system is prepared in the state with $\langle S_z \rangle = -1/2$, the initial value of γ_1 is equal to the number of the vibrational quanta. The physical picture of the transfer process remains the same if one chooses to prepare the initial state with $\langle S_z \rangle = 1/2$.

The dynamics of the vibrational coherence is strongly influenced by the features of the dynamics of the electronic population and coherence. The electronic population dynamics is given by eq 8. The electronic and vibrational coherences are studied below.

2.3. Equations of Motion for the Electronic and Vibrational Coherences. The probe signal (3) is determined by the state-specific positions of the wavepacket and depends on the coherences within the electron-vibrational system. An initial short laser pulse creates both a population imbalance and a coherence between the electronic states. The corresponding operators evolve in time according to the Heisenberg equation $i\hbar\dot{A} = [H, A]$. In particular, the evolution of the electronic coherence operator S_- is given by

$$i\hbar\dot{S}_- = -\Omega S_- - gaS_z \qquad (10)$$

The first term on the right-hand side of eq 10 for the electronic coherence operator is due to purely electronic dynamics. The second term describes the influence of the vibrational subsystem.

The vibrational coherence $\langle a \rangle$ is related to the coordinate of the vibrational wavepacket

$$\langle q \rangle = \sqrt{\hbar/2m\omega}\left(\langle a^+ \rangle + \langle a \rangle\right)$$

and evolves according to

$$i\hbar\dot{a} = -\omega a + gS_- \qquad (11)$$

The equations of motion (EOM) for a and S_- simplify in the interaction picture. An arbitrary operator A is transformed to the interaction representation $\tilde{A}$ by

$$\tilde{A} = \exp(iH_0t/\hbar)\, A \exp(-iH_0t/\hbar) \qquad (12)$$

where $H_0 = \hbar\omega a^+a + \hbar\Omega S_+S_-$ is the interaction-free Hamiltonian; see eq 7. In the interaction representation (12) the electronic and vibrational coherences become

$$\tilde{a}(t) = a(t)e^{-i\omega t}$$
$$\tilde{S}_-(t) = S_-(t)e^{-i\Omega t} \qquad (13)$$

and the EOM (10) and (11) take the form

$$i\hbar\,\dot{\tilde{a}}(t) = g\tilde{S}_- \qquad (14)$$

$$i\hbar\dot{\tilde{S}}_-(t) = -2g\tilde{a}S_z \qquad (15)$$

Upon quantum averaging, eqs 14−15 will be solved by approximating the averages of the products of operators by the products of operator averages, in the spirit of the QHD approach.[51−60] The product closure generates nonlinear coupling between the first-order differential EOM.

2.4. Approximate Solutions to the Equations of Motion for the Coherences. The two first-order differential equations (14) and (15) are equivalent to a single second-order differential equation

$$\frac{d^2}{dt^2}\tilde{a} - \frac{2g^2}{\hbar^2}\tilde{a}S_z = 0 \qquad (16)$$

The expectation value of the electron−nuclear correlation is approximated by the product of the first-order expectation values

$$\langle aS_z \rangle \simeq \langle a \rangle \langle S_z \rangle \qquad (17)$$

It is remarkable that this mean-field description already captures most interference and dephasing effects, in contrast to the Ehrenfest approximation that entirely mistreats the electronic coherence.[78−85]

With identical electronic and vibrational frequencies $\delta = \Omega - \omega = 0$ and $\langle S_z \rangle_{t=0} = -1/2$, eq 8 for the electronic population simplifies to

$$\langle S_z \rangle \simeq -1/4\{\cos\omega'_at + \cos\omega'_bt\} \qquad (18)$$
$$= -1/2\cos\omega_+t\cos\omega_-t$$
$$\omega'_{a,b} = \sqrt{2}g\sqrt{\langle a^+a \rangle \pm \sqrt{\langle a^+a \rangle}}$$
$$\omega_\pm = 1/2(\omega'_a \pm \omega'_b)$$

where $\omega'_{a,b}$ are the simplified expressions for $\omega_{a,b}$, eq 9. The frequencies ω_+, ω_- describe the inversion and quasi-relaxation of the electronic population. The prefix "quasi" indicates that at a later time $t \approx 400\pi$ the system comes close to the initial state. Note that the approximate solution (18) for $\langle S_z\rangle(t)$ includes second-order correlations.[57] Substituting eq 18 into eq 16 for the vibrational amplitude we obtain

$$\ddot{\tilde{a}} + g^2/2\{\cos \omega'_a t + \cos \omega'_b t\}\tilde{a} = 0 \qquad (19)$$

This ordinary linear differential equation with varying coefficients has the same form as the Schrödinger equation for a quasiperiodic potential

$$-\frac{\hbar^2}{2m}\psi'' + [U(X) - E]\,\psi = 0 \qquad (20)$$

with $t \rightarrow X$, $a(t) \rightarrow \psi(X)$, and $\langle S_z\rangle(t) \rightarrow [U(X) - E]$. Equation 20 is also known as the Mathieu equation and was used by Hill to describe moon tides[86] and by Bloch to obtain periodic solid-state wavefunctions.[87]

Equation 19 can be solved numerically. Physically important conclusions may be derived from the approximate perturbative solutions controlled by the electron−phonon coupling constant g. In the zeroth-order, the vibrational coherence remains constant in the interaction picture:

$$\tilde{a}^{(0)}(t) = \tilde{a}(0) = \text{const} \qquad (21)$$

In the first-order, the vibrational coherence oscillates with the same frequency as the electronic population:

$$\tilde{a}^{(1)}(t) = \tilde{a}(0)\left[1 - C + \frac{C}{2}(\cos \omega'_a t + \cos \omega'_b t)\right] \qquad (22)$$

The amplitude of the oscillation is determined by the electron−phonon coupling g and the number of the vibrational quanta $\langle a^+ a\rangle$ at the initial time

$$C = \frac{\omega'^2_a + \omega'^2_b}{2} = 2g^2\langle a^+ a\rangle_{t=0} \qquad (23)$$

The evolution in the interaction picture gives the envelope for the fast oscillation of the vibrational amplitude in the Schrödinger picture

$$a^{(1)}(t) = a(0)\mathrm{e}^{-\mathrm{i}\omega t}\left[1 - C + \frac{C}{2}(\cos \omega'_a t + \cos \omega'_b t)\right] \qquad (24)$$

$$\langle q\rangle(t) = \left(\langle q\rangle(0)\cos \omega t + \frac{\langle p\rangle(0)}{m\omega}\sin \omega t\right)\left[1 - C + \frac{C}{2}(\cos \omega'_a t + \cos \omega'_b t)\right]$$

The exact and approximate perturbative solutions of the simplified eq 19 are compared with the exact quantum evolution in Figure 3. The exact quantum-mechanical expectation value of an observable A

$$\langle A\rangle = \langle\psi(t)|A|\psi(t)\rangle \qquad (25)$$

$$|\psi(t)\rangle = \exp(-\mathrm{i}Ht/\hbar)|\psi(0)\rangle = \sum_j |\phi_j\rangle\langle\phi_j|\psi(0)\rangle \exp(-\mathrm{i}\epsilon_j t/\hbar)$$

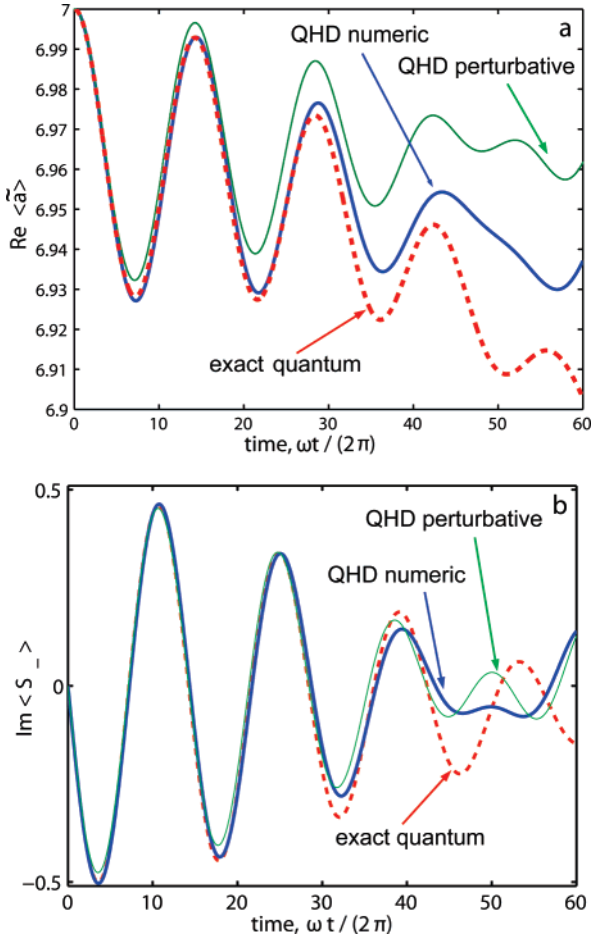

Figure 3. Time evolution of (a) the real part of the vibrational coherence and (b) the imaginary part of the electronic coherence in the interaction picture, determined by exact numeric diagonalization of Hamiltonian (7) (red dashes), numeric solution of eq 19 (blue thick line), and analytic perturbative solution (22) (green thin line) for the same parameter values as in Figure 2. The solutions agree during the first several electronic population transfer events and start to diverge around the first electronic population collapse time[57] $T_{\mathrm{coll}} = \pi/2\omega_-$, corresponding to $\omega T_{\mathrm{coll}}/(2\pi) \simeq 50$. The vibrational and electronic coherences display slowly damped oscillations with the same frequency as the electronic population $\langle S_z\rangle$, Figure 2. The oscillation is small in amplitude, 0.007, compared to the absolute value, 7.

was computed by numeric propagation of the wavefunction, as described in detail in ref 35.

3. Results and Discussion

The evolution of the simplest expectation values $\langle a\rangle$, $\langle S_-\rangle$ is considered first. These expectation values justify the accuracy of the approximations and are used later to build up the time dependence of the probe signal, eq 3. The vibrational a and electronic S_- lowering operators represent the corresponding coherences. At the same time, the real part of $\langle a\rangle$ gives the mean vibrational coordinate. Therefore, $\langle a\rangle$ is also referred to as the vibrational amplitude.

3.1. Evolution of the Vibrational and Electronic Coherences and the Electron-Vibrational Correlation. The expectation values of the vibrational amplitude calculated by the exact wavefunction propagation, numeric solution of the QHD equations, and perturbative solution of the QHD equations are presented in Figure 3a. For all methods, the expectation value of the vibrational amplitude in the interaction representation displays slow damped oscillations of the same frequency as the oscillations of the electronic population $\langle S_z\rangle$. The exact and

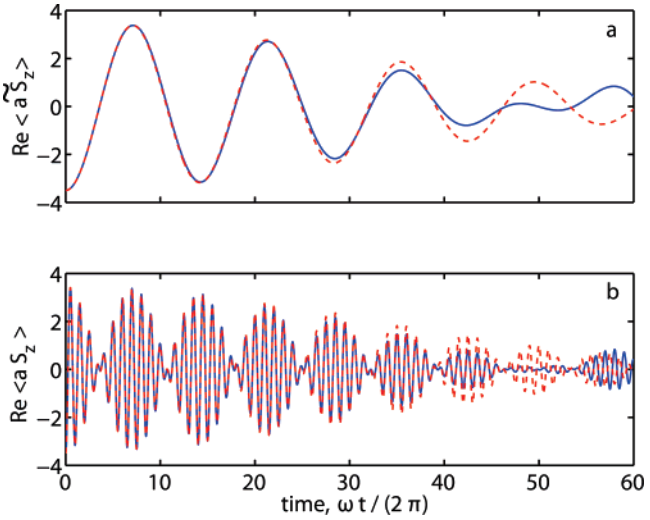

Figure 4. Time dependence of the correlation between the electronic population and vibrational amplitude in (a) the interaction picture and (b) the Schrödinger picture. The interaction representation isolates the key dynamics features, and the Schrödinger representation presents the experimentally observable result. The exact data (blue solid line) are compared with the approximate data (red dashes) generated using eqs 17−19. The results obtained using the perturbative evolution (22) are indistinguishable from the results obtained by numeric integration of eq 19. The initially large electron−phonon correlation decreases with increasing vibrationally induced dephasing in the electronic subsystem.

approximate solutions agree quantitatively for times $\omega t/(2\pi) < 15$ and keep the same qualitative behavior until the time of the first population collapse. Note that, without inhomogeneous broadening, the collapse time coincides with the pure dephasing time.[72] In our model the first population collapse occurs 4 times faster than the population revival[57] $T_{coll} = T_{rev}/4$, $T_{rev} = 2\pi/\omega_-$, such that $\omega T_{coll}/(2\pi) = 49.87$, $T_{coll} \simeq 100\pi$, and $T_{rev} \simeq 400\pi$. The exact solution shows a noticeable decrease in the vibrational amplitude. The decrease is less substantial in the numeric solution of eq 19 and is even smaller in the perturbative solution, eq 22. Note that the oscillations of the vibrational amplitude are small, ≃0.007, relative to its absolute value of ≃7. Although the discrepancy in the oscillations of the mean amplitudes computed by the three methods in the interaction representation $\langle\tilde{a}\rangle(t)$ is noticeable, the observable values of the mean amplitudes given in the Schrödinger representation display negligible differences. The vibrational and electronic coherences given in the interaction representation, Figure 3a,b, provide the envelopes for the rapidly oscillating coherences in the Schrödinger picture (not shown). The coherence transfer of interest is significantly faster than the vibrational relaxation seen in the small decrease of the vibrational amplitude in Figure 3a and is well described by the approximate QHD solutions; see Figures 4 and 5 below.

The dynamics of the vibrational coherence is directly related to the electronic coherence shown in Figure 3b. According to eq 14, the time derivative of the vibrational coherence is proportional to the current magnitude of the electronic coherence. The frequences of the oscillations of the two coherences are determined by the electron−phonon coupling g and the amount of the vibrational energy $\langle a^+a\rangle$, eqs 9 and 18. The envelope of the electronic coherence reaches a maximum each time the populations of the two states become equal. For times shorter than the dephasing time, the exact and QHD solutions show negligible differences. A detailed analysis of electronic-state dynamics in terms of the state projections $\langle S_x\rangle$, $\langle S_y\rangle$, and $\langle S_z\rangle$ on the Bloch sphere is given in ref 57.

The evolution of the correlation between the vibrational coherence and electronic population $\langle aS_z\rangle$ is plotted in Figure 4. The approximate solutions are obtained using closure (17) and eqs 18 and 19. The approximate correlation $\langle a\rangle\langle S_z\rangle$ generated by solving eq 19 numerically is indistinguishable from the result obtained with the perturbation theory (22). The approximate results (solid line) agree with the exact solution (dashes), Figure 4.

In the interaction picture, the correlation $\langle\widetilde{aS_z}\rangle$ shown in Figure 4a oscillates with the same frequency as the electronic population $\langle S_z\rangle$ shown in Figure 2. The maximum value of $\langle\widetilde{aS_z}\rangle$ is equal to half of the maximum value of $\langle\tilde{a}\rangle$. The electron-vibrational correlation is high initially and decreases due to dephasing. The correlation in the Schrödinger picture rapidly oscillates with the vibrational frequency ω, Figure 4b. Similar to the observables shown in Figures 2 and 3, the QHD solutions given in Figure 4 agree quantitatively with the exact solutions until $\omega t/(2\pi) < 15$ and are qualitatively correct up to the collapse time $\omega T_{coll}/(2\pi) \simeq 50$. Because $\langle a\rangle$, $\langle S_-\rangle$, and $\langle aS_z\rangle$ are complex variables, Figures 3 and 4 display their real or imaginary parts, corresponding to $\langle q\rangle\sqrt{2m\omega/\hbar}$, $\langle S_y\rangle$, and $\langle qS_z\rangle\sqrt{2m\omega/\hbar}$. The complementary variables $\langle p\rangle\sqrt{2/m\omega\hbar}$, $\langle S_x\rangle$, and $\langle pS_z\rangle\sqrt{2/m\omega\hbar}$ exhibit similar behavior.

3.2. State-Specific Vibrational Coherence Operators. The vibrational coherence transfer can be conveniently analyzed using linear combinations of the electron-vibrational correlation $\langle aS_z\rangle$ and the vibrational coherence $\langle a\rangle$. Using completeness in the electronic subsystem $\hat{1}_{el} = |1\rangle\langle 1| + |1'\rangle\langle 1'|$, the vibrational coherence $\langle a\rangle$ can be written in the total electron-vibrational space as

$$\langle a\rangle = \langle a\cdot\hat{1}_{el}\rangle = \langle a(|1'\rangle\langle 1'| + |1\rangle\langle 1|)\rangle$$

Combinations of the electronic population S_z and the unit $\hat{1}_{el}$ operator give projections onto the initial $|1\rangle\langle 1|$ and final $|1'\rangle\langle 1'|$ electronic states. Similarly, combinations of the correlation $\langle aS_z\rangle$ and vibrational coherence $\langle a\hat{1}_{el}\rangle$ give the expectation values of the vibrational coherences for the initial $\langle a|1\rangle\langle 1|\rangle$ and final $\langle a|1'\rangle\langle 1'|\rangle$ electronic states

$$\langle a|1\rangle\langle 1|\rangle = \langle a\hat{1}/2 + aS_z\rangle \qquad (26)$$
$$\langle a|1'\rangle\langle 1'|\rangle = \langle a\hat{1}/2 - aS_z\rangle$$

The state-specific vibrational coherence operators characterize the location of the vibrational wavepacket, correlated with a given electronic state. The real parts of (26) represent the state-specific coordinates, and the imaginary parts represent the state-specific momenta. The values of the state-specific vibrational coordinates determine the magnitude of the probe signal (3).

3.3. Pathways of the Vibrational Coherence. Consider the evolution of the expectation values of the state-specific vibrational coherences (26) for the system prepared in a direct product of pure electronic and coherent quasiclassical vibrational states.

$$|\psi\rangle = \underset{\text{vibrational}}{|\alpha\rangle} \cdot \underset{\text{electronic}}{|1\rangle} \qquad (27)$$

Figure 5 shows the dynamics of the state-specific vibrational coordinates corresponding to this situation. Initially $\langle S_z\rangle_{t=0} = -1/2$, and the expectation value $\langle q|1'\rangle\langle 1'|\rangle_{t=0}$ specific for the final state is zero. The initial vibrational amplitude $\langle a|1\rangle\langle 1|\rangle_{t=0}$ in the initial state coincides with the total amplitude $\langle a\rangle_{t=0}$, which

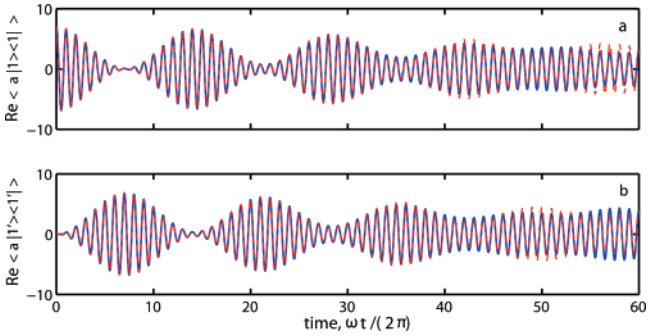

Figure 5. Time dependence of the state-specific vibrational coordinates for (a) the initial and (b) the final electronic state. The exact data (blue solid line) are compared with the approximate results (red dashes) generated using eqs 18 and 19. The results obtained using the numeric solution of eq 19 are indistinguishable from the results obtained using perturbation theory solution (22). The vibrational coordinate associated with the final state starts at zero. The vibrational coordinate associated with the initial state starts equal to the overall vibrational coordinate and oscillates with the vibrational frequency ω. The dynamics of the state-specific vibrational coordinates are correlated with the electronic population dynamics, Figure 2.

oscillates with the frequency corresponding to the electronic state $|1\rangle$; see Figure 1.

The electronic evolution affects the vibrational subsystem. As the electronic subsystem approaches the first population flip, the vibrational amplitude of the initial state decreases quickly, and the amplitude of the final state rises, Figure 5. When the electronic population $\langle S_z \rangle$ changes sign and reaches $^1/_2$, the initial-state vibrational coherence vanishes, and the final-state vibrational coherence grows to the maximal value equal to the total vibrational amplitude. This transfer of the vibrational coherence between the electronic states repeats multiple times and is very well described by the QHD approximation.

The fact that the simple QHD approximation involving the first-order closure (17) gives good agreement with the exact result is remarkable and emphasizes the flexibility of the QHD approach. If the operator representation is chosen appropriately, higher order QHDs are not needed. The lowest-order mean-field-type approximation becomes sufficient and can be easily used in practice for large systems.

In the wavefunction representation, the vibrational coherence transfer involves motion of the vibrational wavepacket between the electronic potential energy surfaces; see eq 2 and Figure 1. In some cases, the transfer of the electronic population and the vibrational coherence show distinct steps.[10,11,28,88] In the present case the transfer is continuous, because the initial vibrational amplitude is much larger than the displacement between the potential energy minima in the two electronic states. First, the larger portion of the wavepacket remains in the initial potential, and the expectation value of the vibrational coordinate oscillates around the equilibrium position of the initial surface. Gradually, the wavepacket shifts to the final state, and its mean coordinate oscillates around the equilibrium position associated with the final state. If the curvatures of the initial and final electronic energy surfaces are different, the frequency of the oscillation of the vibrational coordinate changes during the transfer.

Experimentally, emission from the excited states $|1\rangle$ and $|1'\rangle$ to the ground state $|0\rangle$ may be induced by a short probe pulse, which is characterized by frequency and arrival time. The transition will occur only if the pulse frequency matches the energy gap between the ground and excited electronic states at the pulse arrival time. Because the energy gap is modulated by the evolution of the vibrational wavepacket, Figure 1, the optimal probe frequency is determined by the wavepacket coordinate. In the majority of experiments performed using a constant probe frequency, a mismatch between the optimal and experimental probe frequencies decreases the signal intensity. The signal intensity analysis performed with the time-window Fourier transform technique is able to reveal the vibrational coherence transfer between the electronic states with different potential energy curvatures.[89] The recently observed[6,20,23,61,62] effect of vibrational coherence transfer is distinct from the more typical transfers of electronic energy and population, during which vibrational coherence is usually not maintained.

4. Concluding Remarks

Vibrational coherence transfer is an important and fascinating effect observed in a variety of systems, including natural and artificial light-harvesting complexes, proteins, and liquids.[6,20,23,61,62] Closely related to the energy and electron transfer, the vibrational coherence transfer is a separate phenomenon that occurs on the time scale of the electronic transition. To be observed, the transfer of vibrational coherence must proceed faster than dephasing. On the other hand, the energy and electron transfer can be incoherent and slower than dephasing.

The vibrational coherence transfer has been described with the QHD approach at a very simple, but accurate level. Good agreement between the exact quantum simulation and QHD involving the first-order closure (17) is an outstanding result, emphasizing the value of proper representation of the physical phenomenon. In contrast, the Ehrenfest approach, which also involves the first-order closure,[52] is formulated with a different set of operators and grossly mistreats quantum coherence.[78−85] The results reported here and in the previous publication[57] indicate that spin-phonon models are particularly useful for quantum description of population and coherence transfer, dephasing, and relaxation.

The presented results are obtained with a minimalistic approach that can be extended with great computational efficiency to systems comprised of many vibrational and electronic degrees of freedom. The current level of the QHD approximation extends only one step beyond classical mechanics. The number of the first-order equations involved in the approximation scales quadratically with system dimensionality N, and so does the computational effort. In comparison, an exact wavefunction method requires propagation in the space of M^N basis vectors with M vectors per degree of freedom, and a density matrix description scales as M^{2N}. The presented approach can be applied to systems that are nearly the same in size as those described with classical mechanics, allowing for a great level of detail in the modeling of the experimental data.

Acknowledgment. We thank V. Nagarajan, W. W. Parson, Yu. V. Pereverzev, C. F. Craig, and E. I. Zenkewich for useful discussions. The research was supported by NSF Grant No. CHE-0701517 and ACS-PRF Grant No. 46772-AC6. O.V.P. acknowledges support of the JSPS Fellowship for Foreign Scholars and is grateful to Professor Yoshitaka Tanimura at Kyoto University for hospitality during manuscript preparation.

References and Notes

(1) Fleming, G. R.; Scholes, G. D. *Nature* **2004**, *431*, 256.
(2) Green, B. R.; Parson, W. W. *Light-Harvesting Antennas in Photosynthesis*; Kluwer: Dordrecht, The Netherlands, 2003.
(3) van Amerongen, H.; Valkunas, L.; van Grondelle, R. *Photosynthetic Excitons*; World Scientific: NJ, 2000.
(4) Vos, M. H.; Rischel, C.; Jones, M.; Martin, J.-L. *Biochemistry* **2000**, *39*, 2687.
(5) Cogdell, R. J.; Gardiner, A. T.; Roszak, A. W.; Law, C. J.; Southall, J.; Isaacs, N. W. *Photosynth. Res.* **2004**, *81*, 207.

(6) Parson, W. W.; Warshel, A. *Chem. Phys.* **2004**, *296*, 201.
(7) Novoderezhkin, V. I.; Yakovlev, A. G.; van Grondelle, R.; Shuvalov, V. A. *J. Phys. Chem. B* **2004**, *108*, 7445.
(8) Zenkevich, E. I.; Kilin, D. S.; Willert, A.; Bachilo, S. M.; Shulga, A. M.; Remel, U.; v. Borczyskowski, C. *Mol. Cryst. Liq. Cryst.* **2001**, *361*, 83.
(9) Zenkevich, E. I.; Willert, A.; Bachilo, S. M.; Rempel, U.; Kilin, D. S.; Shulga, A. M.; von Borczyskowski, C. *Mater. Sci. Eng. C* **2001**, *18*, 99.
(10) Ramakrishna, S.; Willig, F.; May, V. *Phys. Rev. B* **2000**, *62*, R16330.
(11) Ramakrishna, S.; Willig, F.; May, V. *J. Chem. Phys.* **2001**, *115*, 2743.
(12) Zenkevich, E. I.; Cichos, F.; Shulga, A.; Petrov, E. P.; Blaudeck, T.; von Borczyskowski, C. *J. Phys. Chem. B* **2005**, *109*, 8679.
(13) Asbury, J. B.; Anderson, N. A.; Hao, E. C.; Ai, X.; Lian, T. Q. *J. Phys. Chem. B* **2003**, *107*, 7376.
(14) Zimmermann, C.; Willig, F.; Ramakrishna, S.; Burfeindt, B.; Pettinger, B.; Eichberger, R.; Storck, W. *J. Phys. Chem. B* **2001**, *105*, 9245.
(15) Stier, W.; Prezhdo, O. V. *J. Phys. Chem. B* **2002**, *106*, 8047.
(16) Stier, W.; Prezhdo, O. V. *Isr. J. Chem.* **2003**, *42*, 213.
(17) Stier, W.; Duncan, W. R.; Prezhdo, O. V. *Adv. Mat.* **2004**, *16*, 240.
(18) Duncan, W. R.; Prezhdo, O. V. *J. Phys. Chem. B* **2005**, *109*, 365.
(19) Duncan, W. R.; Stier, W.; Prezhdo, O. V. *J. Am. Chem. Soc.* **2005**, *127*, 7941.
(20) Khalil, M.; Demirdoven, N.; Tokmakoff, A. *J. Chem. Phys.* **2004**, *121*, 362.
(21) Gruebele, M. *J. Phys. Condens. Matt.* **2004**, *16*, R1057.
(22) Cina, J. A.; Fleming, G. R. *J. Phys. Chem. A* **2004**, *108*, 11196.
(23) Scheurer, C.; Mukamel, S. *J. Chem. Phys.* **2002**, *116*, 6803.
(24) Mukamel, S. *Annu. Rev. Phys. Chem.* **2000**, *51*, 691.
(25) Shi, Q.; Geva, E. *J. Chem. Phys.* **2004**, *120*, 10647.
(26) Shi, Q.; Geva, E. *J. Chem. Phys.* **2003**, *119*, 11773.
(27) Schreiber, M.; Kilin, D.; Kleinekathöfer, U. *J. Lumin.* **1999**, *83&84*, 235.
(28) Cina, J. A.; Kilin, D. S.; Humble, T. S. *J. Chem. Phys.* **2003**, *118*, 46.
(29) Humble, T. S.; Cina, J. A. *Phys. Rev. Lett.* **2004**, *93*, 060402.
(30) Förster, T. in *Modern Quantum Chemistry*; Sinanoglu, O., Ed.; Academic Press: New York, 1965; p 93.
(31) Marcus, R. A. *J. Chem. Phys.* **1956**, *24*, 966.
(32) Marcus, R. A. *Rev. Mod. Phys.* **1993**, *65*, 599.
(33) Small, D. W.; Matyushov, M. V.; Voth, G. A. *J. Am. Chem. Soc.* **2003**, *125*, 7470.
(34) Marcus, R. A.; Sutin, N. *Biochim. Biophys. Acta* **1985**, *2*, 65.
(35) Kilin, D.; Kleinekathöfer, U.; Schreiber, M. *J. Phys. Chem. A* **2000**, *104*, 5413.
(36) Gruebele, M.; Wolynes, P. G. *Acc. Chem. Res.* **2004**, *37*, 261.
(37) Schröder, M.; Kleinekathöfer, U.; Schreiber, M. *J. Chem. Phys.* **2006**, *124*, 084903.
(38) Welack, S.; Schreiber, M.; Kleinekathöfer, U. *J. Chem. Phys.* **2006**, *124*, 044712.
(39) Yang, S.; Cao, J. *J. Chem. Phys.* **2002**, *121*, 562.
(40) Kondov, I.; Kleinekathöfer, U.; Schreiber, M. *J. Chem. Phys.* **2003**, *119*, 6635.
(41) Schreiber, M.; Herman, P.; Barvik, I.; Kondov, I.; Kleinekathöfer, U. *J. Lumin.* **2004**, *108*, 137.
(42) Kleinekathöfer, U. *J. Chem. Phys.* **2004**, *121*, 2505.
(43) Kleinekathöfer, U.; Schröder, M.; Schreiber, M. *J. Lumin.* **2005**, *112*, 461.
(44) Prezhdo, O. V.; Rossky, P. J. *J. Phys. Chem.* **1996**, *100*, 17094.
(45) Mosyak, A. A.; Prezhdo, O. V.; Rossky, P. J. *J. Chem. Phys.* **1998**, *109*, 6390.
(46) Brooksby, C.; Prezhdo, O. V.; Reid, P. J. *J. Chem. Phys.* **2003**, *118*, 4563.
(47) Brooksby, C.; Prezhdo, O. V.; Reid, P. J. *J. Chem. Phys.* **2003**, *119*, 9111.
(48) Matyushov, D. V. *J. Chem. Phys.* **2004**, *120*, 7532.
(49) Matyushov, D. V. *J. Chem. Phys.* **2005**, *122*, 044502.
(50) Tully, J. C. In *Classical and Quantum Dynamics in Condensed Phase Simulations*; Berne, B. J., Ciccotti, G., Coker, D. F., Eds.; World Scientific: NJ, 1998.
(51) Pereversev, Y. V.; Prezhdo, O. V. *J. Chem. Phys.* **2000**, *113*, 6557.
(52) Brooksby, C.; Prezhdo, O. V. *Chem. Phys. Lett.* **2001**, *346*, 463.
(53) Prezhdo, O. V. *J. Chem. Phys.* **2002**, *117*, 2995.
(54) Prezhdo, O. V.; Pereverzev, Y. V. *J. Chem. Phys.* **2002**, *116*, 4450.
(55) Pahl, E.; Prezhdo, O. V. *J. Chem. Phys.* **2002**, *116*, 8704.
(56) Brooksby, C.; Prezhdo, O. V. *Chem. Phys. Lett.* **2003**, *378*, 533.
(57) Kilin, D. S.; Pereverzev, Y. V.; Prezhdo, O. V. *J. Chem. Phys.* **2004**, *120*, 11209.
(58) Heatwole, E.; Prezhdo, O. V. *J. Chem. Phys.* **2004**, *121*, 10967.
(59) Heatwole, E.; Prezhdo, O. V. *J. Chem. Phys.* **2005**, *122*, 234109.
(60) Prezhdo, O. V. *Theor. Chem. Acc.* **2006**, *116*, 206.
(61) Kim, Y. S.; Hochstrasser, R. M. *J. Phys. Chem. B* **2006**, *110*, 8531.
(62) Johnson, E. T.; Nagarajan, V.; Zazubovich, V.; Riley, K.; Small, G. J.; Parson, W. W. *Biochemistry* **2003**, *42*, 13673.
(63) Zazubovich, V.; Tibe, I.; Small, G. J. *J. Phys. Chem. B* **2001**, *105*, 12410.
(64) Nagarajan, V.; Parson, W. W. *J. Chem. Phys. B* **2000**, *104*, 4010.
(65) Nagarajan, N.; Johnson, E. T.; Williams, J. C.; Parson, W. W. *J. Chem. Phys. B* **1999**, *103*, 2297.
(66) Gelin, M. F.; Egorova, D.; Domcke, W. *Chem. Phys.* **2004**, *301*, 129.
(67) Streltsov, A. M.; Vulto, S. I. E.; Shkuropatov, A. Y.; Hoff, A. J.; Aartsma, T. J.; Shuvalov, V. A. *J. Phys. Chem. B* **1998**, *102*, 7293.
(68) Shuvalov, V. A.; Yakovlev, A. G. *FEBS Lett.* **2003**, *26*, 540.
(69) Schatz, G. C.; Ratner, M. A. *Quantum Mechanics in Chemistry*; Prentice Hall: Englewood Cliffs, NJ, 1993.
(70) Milliron, D. J.; Hughes, S. M.; Cui, Y.; Manna, L.; Li, J. B.; Wang, L. W.; Alivisatos, A. P. *Nature* **2004**, *430*, 190.
(71) Klimov, V. I.; Mikhailovsky, A. A.; Xu, S.; Malko, A.; Hollingsworth, J. A.; Leatherdale, C. A.; Eisler, H. J.; Bawendi, M. G. *Science* **2000**, *290*, 314.
(72) Kamisaka, H.; Kilina, S. V.; Yamashita, K.; Prezhdo, O. V. *Nano Lett.* **2006**, *6*, 2295.
(73) Bachilo, S. M.; Strano, M. S.; Kittrell, C.; Hauge, R. H.; Smalley, R. E.; Weisman, R. B. *Science* **2002**, *298*, 2361.
(74) Habenicht, B. F.; Craig, C. F.; Prezhdo, O. V. *Phys. Rev. Lett.* **2006**, *96*, 187401.
(75) Tretiak, S.; Kilina, S.; Piryatinski, A.; Saxena, A.; Martin, R. L.; Bishop, A. R. *Nano Lett.* **2007**, *7*, 86.
(76) Zheng, J. R.; Kang, Y. K.; Therien, M. J.; Beratan, D. N. *J. Am. Chem. Soc.* **2005**, *127*, 11303.
(77) Guldi, D. M.; Swartz, A.; Luo, C. P.; Gomez, R.; Segura, J. L.; Martin, N. *J. Am. Chem. Soc.* **2002**, *124*, 10875.
(78) Bittner, E. R.; Rossky, P. J. *J. Chem. Phys.* **1995**, *103*, 8130.
(79) Prezhdo, O. V.; Rossky, P. J. *J. Chem. Phys.* **1997**, *107*, 5863.
(80) Prezhdo, O. V.; Rossky, P. J. *Phys. Rev. Lett.* **1998**, *81*, 5294.
(81) Prezhdo, O. V. *J. Chem. Phys.* **1999**, *111*, 8366.
(82) Prezhdo, O. V. *Phys. Rev. Lett.* **2000**, *85*, 4413.
(83) Hack, M. D.; Truhlar, D. G. *J. Chem. Phys.* **2001**, *114*, 9305.
(84) Zhu, C. Y.; Jasper, A. W.; Truhlar, D. G. *J. Chem. Phys.* **2004**, *120*, 5543.
(85) Zhu, C. Y.; Nangia, S.; Jasper, A. W.; Truhlar, D. G. *J. Chem. Phys.* **2004**, *121*, 7658.
(86) Mathews, R. L. W. J. *Mathematical Methods of Physics*; Benjamin: New York, 1965.
(87) Kittel, C. *Introduction to Solid State Physics*; J. Wiley: New York, 1996.
(88) Kilin, D. S.; Cina, J. A.; Prezhdo, O. V. Preprint quant-ph/0412219, 2005.
(89) Dao, L. V. *J. Lumin.* **2004**, *106*, 243.